Persistent patterns and multifractality in fluid mixing

Bala Sundaram,[1] Andrew C. Poje,[2] and Arjendu K. Pattanayak[3]
[1]*Department of Physics, University of Massachusetts, 100 Morrissey Boulevard, Boston, Massachusetts 02125, USA*
[2]*Department of Mathematics and Graduate Faculty in Physics, City University of New York-CSI, Staten Island, New York 10314, USA*
[3]*Department of Physics and Astronomy, Carleton College, Northfield, Minnesota 55057, USA*
(Received 23 December 2008; revised manuscript received 12 May 2009; published 5 June 2009)

Persistent patterns in periodically driven dynamics have been reported in a wide variety of contexts ranging from table-top and ocean-scale fluid mixing systems to the weak quantum-classical transition in open Hamiltonian systems. We illustrate a common framework for the emergence of these patterns by considering a simple measure of structure maintenance provided by the average radius of the scalar distribution in transform space. Within this framework, scaling laws related to both the formation and persistence of patterns in phase space are presented. Further, preliminary results linking the scaling exponents associated with the persistent patterns to the multifractal nature of the advective phase-space geometry are shown.

DOI: 10.1103/PhysRevE.79.066202 PACS number(s): 05.45.−a, 47.52.+j, 47.54.−r, 83.50.Xa

I. INTRODUCTION

The role of chaotic dynamics in assisting the mixing of a passive scalar is of broad interest with applications ranging from micromixers to chemical reactors to geophysical tracer transport. These dynamics are a stirring mechanism, which conventional wisdom suggests facilitates the mixing process [1]. The evolution of a passive scalar field is described by the advection-diffusion equation

$$\frac{\partial C}{\partial t} + \vec{u} \cdot \vec{\nabla} C = D \nabla^2 C, \tag{1}$$

where $C(\vec{x},t)$ is the concentration, D is the (constant) diffusivity, and $\vec{u}$ is the prescribed Eulerian velocity. The two processes of advective mixing and diffusion work very differently: stretching and folding by the chaotic velocity field rapidly sharpens concentration gradients, while diffusion acts to smooth these gradients. As a result, the competition between the two can lead to counterintuitive results. In particular, a number of experimental and numerical investigations [2–7] has shown that the long-time dynamics of the scalar field under the action of time-periodic chaotic advection is itself time periodic (after appropriate rescaling of the variance) and is completely determined by the slowest decaying Floquet mode of the corresponding single period advection-diffusion (Poincaré) operator. This "strange eigenmode" [2] is characterized by exponential decay of the scalar variance and self-similar evolution of both the scalar spectrum and probability distribution. Studies of these patterns show that regions of high concentration gradients of the passive scalar are associated with features of the underlying chaos in the Lagrangian dynamics, specifically the unstable manifolds of the fixed points of associated Poincaré maps [4] and the boundaries of integrable regions of the flow produced by the presence of Kolmogorov-Arnold-Moser tori [7].

Interest in the nature of such persistent patterns, extends beyond fluid dynamics and mixing. Specifically, Eq. (1) in even dimensions corresponds to the dynamics of a classical probability density in the presence of noise. The dynamics of the relaxation of such densities to equilibrium is of relevance to the foundations of statistical mechanics. Further, the rate of decay of gradients in classical probabilities strongly influences the difference between quantum and classical evolutions, thus making these patterns of interest in quantum-classical correspondence [8] as well.

Specific questions concerning what sets the overall decay rate of the persistent pattern and how this decay rate scales with both the diffusivity and parameters in the velocity field have been addressed in a number of flows, typically those representable by discrete two-dimensional (2D) maps. The range of validity of local theories based on the distribution of stretching rates in the chaotic field [9,10] has been investigated for homogeneous or nearly homogeneous maps [5,11–13]. Direct calculation of the spectral properties of the Poincaré operator of the advection-diffusion equation for maps with mixed phase-space dynamics has shown that the degree of spatial localization of eigensolutions, the scaling of the spectrum with diffusivity and the existence of degenerate states are intimately connected with fine-scale details of the underlying phase-space geometry [7,14].

In this paper we examine the connection between measurable statistical properties of the geometry of the advective dynamics and the scaling of a previously proposed, easily computed, measure of pattern strength [15]. This measure, defined by the Dirichlet quotient of the scalar energy, $L_2(t) = \int |C(\vec{x},t)|^2 d\vec{x}$, and enstrophy, $C_2(t) = \int |\nabla C(\vec{x},t)|^2 d\vec{x}$,

$$\chi^2(t) = \frac{C_2(t)}{L_2(t)} = \frac{\int |\vec{k}|^2 |C(\vec{k},t)|^2 d\vec{k}}{\int |C(\vec{k},t)|^2 d\vec{k}}, \tag{2}$$

explicitly tracks the competition between advective and diffusive effects. Physically, $\chi^2(t)$ measures the mean-square radius of the scalar distribution in k space, reflecting the distance between the largest stirring scales and the smallest length scales at which advection can produce structure in the presence of smoothing. Previous analysis [15] concentrated on uniformly hyperbolic chaotic systems, where it was shown that $\chi^2(t)$ initially grows as the dynamics produces structure, reaches a plateau (which scales as D^{-1}) due to a balance between the dynamics and diffusion, and then

abruptly decays to zero as diffusion overtakes the spatially homogeneous dynamics. This latter behavior is peculiar to uniform hyperbolicity and explains why no persistent patterns are possible in that case.

Similar analyses are extended here to study the balance between chaos and diffusion in non-uniformly-hyperbolic systems including those with mixed phase-space dynamics. As we show in the next section, for spatially inhomogeneous advecting fields, χ^2 goes through distinct dynamical stages before approaching a nonzero saturation value χ^2_∞. This saturated value of χ^2 is a clear indicator of the emergence of persistent patterns with self-similar evolution of the scalar spectrum and identical decay rates for both the scalar variance and the gradient norm.

In the third section, we examine how the time-asymptotic value of this measure scales with both the diffusivity and the chaoticity parameter for dynamics driven by the standard map. Unlike fully mixing, uniformly hyperbolic flows where semianalytic arguments lead to D^{-1} scaling of χ^2 on intermediate time scales, typical chaotic dynamics produce structure on multiple space scales. The multiscale distribution of stretching rates is found to result in the power-law scaling, $\chi^2_\infty \simeq D^{-\gamma}$. The scaling exponent γ exhibits both a sensitive dependence on geometric details of the chaotic transport as measured by the multifractality of the chaotic partition of the phase space [16], as well as diffusivity dependence shown to be related to the size of integrable islands in the flow. This behavior is arguably universal and is confirmed by similar analysis of a continuous-in-time flow field. We also explore variations seen in the exponent γ, under certain conditions, suggesting the role of local phase-space structures in influencing the pattern formation over different ranges of the diffusivity.

Finally, we briefly touch on the issue of relating γ to phase-space measures which account for the presence of diffusion (or noise in a dynamical sense) by considering a finite-time version of the Hausdorff measure [17], $H_D(t)$. The time at which this measure is computed is set by an estimate of the time, t^*, when the diffusive term terminates advective structure formation on finer scales. This characteristic time scale is well short of saturation but ultimately affects variation in stretching rates and, hence, the persistent patterns seen. Though we are not able to extract a definitive relationship, our results show indications of a relationship of the type $\gamma \approx H_D(t^*) - 1$. We conclude with a summary, including prospects for future research.

II. DYNAMICAL STAGES IN THE FORMATION OF PERSISTENT PATTERNS

To illustrate our arguments, we consider the dynamics associated with the standard or Chirikov-Taylor map described by the Hamiltonian

$$H(p,q,t) = \frac{p^2}{2} + K \cos q \sum_n \delta(t-n), \tag{3}$$

with unit temporal spacing between the δ kicks. The dynamics in this case are defined on a toroidal geometry (periodic boundary conditions in both p,q). This system exhibits generic mixed phase-space dynamics for a wide range of K, which controls the variation in hyperbolicity. A classical probability or Liouville density evolves in a Fourier basis $\exp[2\pi i(np+mq)]$ as

$$\rho^{t+1}_{m,n} = \sum_k J_{m-k}(nK)\rho^t_{k,k+n} \exp[-D(m^2+n^2)], \tag{4}$$

where J_s is the Bessel function of sth order, and the role of the diffusion is captured in the term-by-term decay of the Fourier elements. We reiterate that the dynamics of this phase-space Liouville density maps precisely to the real-space behavior of a two-dimensional fluid.

We begin from the integrable free-particle limit, corresponding to $K=0$. One reason for considering an integrable case is that it corresponds to a subset of initial conditions in the situation of mixed phase-space dynamics, and as such it is important to be able to show that any proposed diagnostic for persistent patterns can pick these regions out. A second reason will become clear shortly, when we show that the decay in the $L2$ norm can deceptively signal the presence of persistent patterns.

For $K=0$ the Fourier space propagator reduces to a delta function $J_{m-k}=\delta_{m,k}$. With the initial condition $\rho^0_{m,n}=\rho^0_{-m,-n}=\delta_{m,1}\delta_{n,-1}$, which has gradients in both p and q, the dynamical evolution is completely determined by

$$\rho^{t+1}_{m,n} = \rho^t_{m,m+n} \exp[-D(m^2+n^2)], \tag{5}$$

leading to the solution

$$\rho^t_{m,n} = \left[\exp\ -D\left(t + \sum_{n=2}^{t+1} n^2\right)\right][\delta_{m,1}\delta_{n,-t-1} + \delta_{m,-1}\delta_{n,t+1}] \tag{6}$$

with norms $L_2(t)=2\exp\{-2Dt[1+\beta(t)]\}$ and $C_2(t)=[(t+1)^2+1]L_2(t)$, where $\beta(t)=(8t^2+15t+19)/6$. This implies that $\chi^2(t)=t^2+2t+2$, independent of the diffusion coefficient D.

Note that this integrable solution has superexponential decay of L_2, which is usually associated with the absence of persistent patterns. However, as we now see, the choice of a different initial condition can change this. This is due to the fact that $K=0$ corresponds to a simple shear flow in q. Choosing an initial condition $\rho^0_{m,n}=\rho^0_{-m,-n}=\delta_{m,0}\delta_{n,1}$ with gradients only in the p direction, it is easy to show that

$$\rho^t_{m,n} = \exp[-D(m^2+n^2)t][\delta_{m,0}\delta_{n,1} + \delta_{m,0}\delta_{n,-1}]. \tag{7}$$

In this instance, we get the simpler (and intuitively obvious) result that $L_2(t)=C_2(t)=2\exp[-2Dt]$ and therefore $\chi^2(t)=1$. It should now be noted that, based on initial conditions, both exponential and superexponential decays of the L_2 norm were obtained although neither situation results in the formation of persistent patterns.

Moving away from the integrable limit, that is, for the parameter range $0<K\ll 1$, shown in Fig. 1 along with the $K=0$ case, we see that χ^2 initially follows the quadratic growth associated with integrable dynamics followed by an abrupt fall-off to a lower value which slowly decays. This sharp decline is similar to that for uniformly hyperbolic dynamics ($K\gg 1$) where diffusion effectively homogenizes the

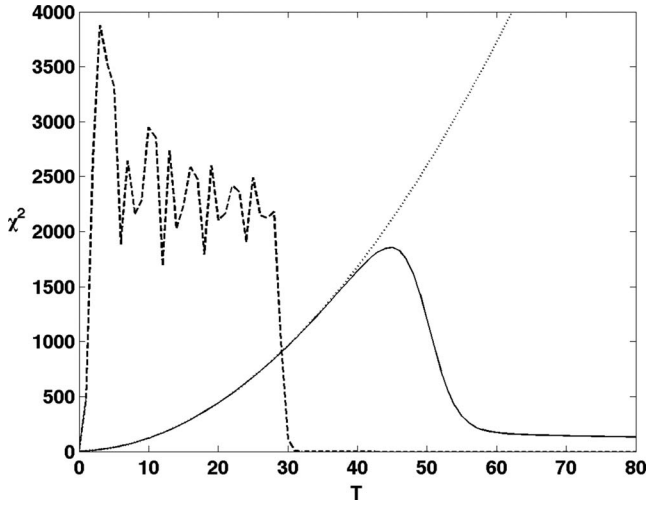

FIG. 1. The two extremes of near-integrable behavior where $K=10^{-4}$ (solid line) and near uniform hyperbolicity for $K=100$ (dashed line) are contrasted. $D=10^{-4}$ in both cases. Analytic, $K=0$ shown in dotted line.

concentration once the spacing between high-density regions falls within the single period diffusive length scale. By contrast, as we now see, in the near-integrable case, the spacing remains nonuniform resulting in the slow (linear) removal of residual gradients.

For intermediate values of K we note that while the phase space of the standard map is "mixed" for all finite values of K, the size of the integrable island structures vanishes rapidly as $K\to\infty$. Since the diffusivity effectively homogenizes dynamics on scales $l\sim\sqrt{D}$, there exist values of D, for large values of K, where the scalar dynamics is essentially characterized by the non-uniformities in the hyperbolic partition of the phase space and not on the dynamics in integrable regions or the details of the boundary layers surrounding such structures.

Figure 2(a) shows the behavior of $\chi^2(t)$ for several values of K for a single initial condition which extends over the entire phase space. In each case, four distinct regions are seen: (A) where the dynamics dominate and structure is produced on ever finer scales (χ^2 increasing rapidly), followed by (B) the onset of the diffusive counterthrust which smoothes gradients and removes structure starting from the smallest scales (χ^2 stops growing), and then (C) a regime of decreasing χ^2 where diffusion has now overtaken the dynamics until (D) a balance is reached between the influences of dynamics and diffusion where $\chi^2(t)$ attains a "saturation" value. As shown in Figs. 2(b) and 2(c), this last plateau region for $\chi^2(t)$ corresponds to a quasistationary, persistent pattern in the concentration field where L_2 and C_2 decay at identical rates. These patterns clearly display both the stable island regions, if any exist, as well as the features of the unstable manifold. Both the maximum of χ^2 curve as well as

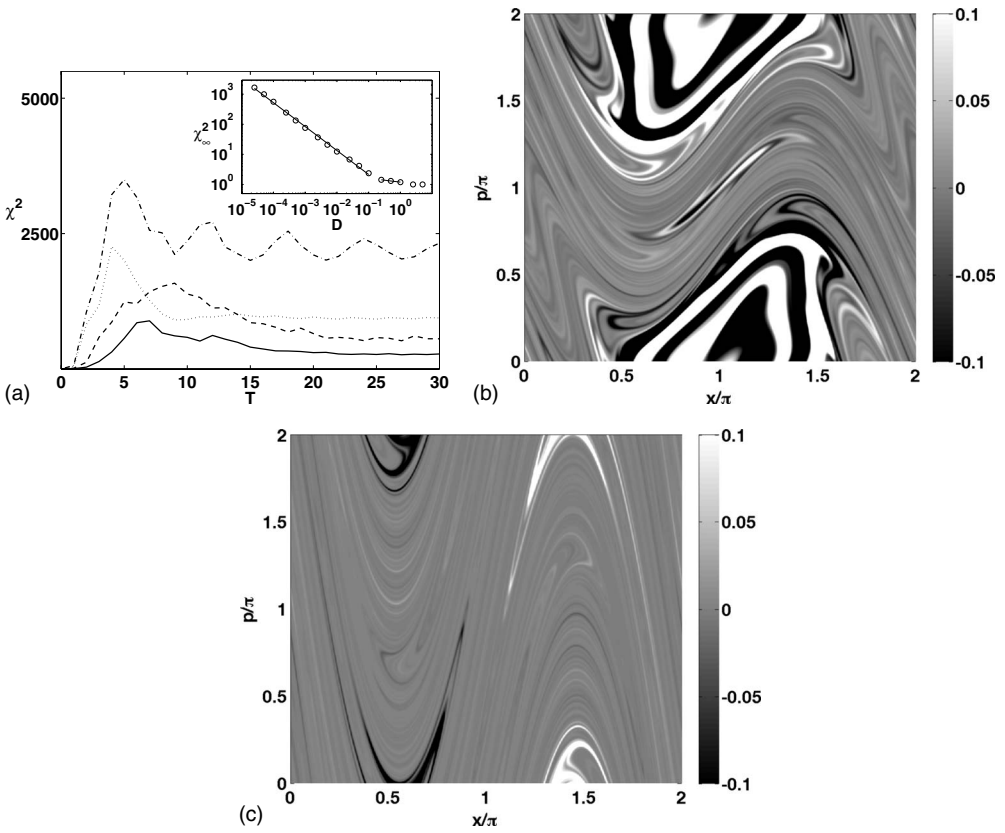

FIG. 2. (a) $\chi^2(t)$ for mixed phase-space dynamics. $K=2.1$ (solid), $K=3.5$ (dashed), $K=7$ (dotted), and $K=8$ (dot-dashed). $D=10^{-4}$ in each case. Note that all the curves go through the stages (a) rapid increase, (b) turnover, (c) decrease, and (d) steady state. Inset: saturation value of χ^2 as a function of D for $K=7$. (b) Persistent pattern for $K=2.1$ and $t=30$. (c) Persistent pattern for $K=7$ at $t=30$.

TABLE I. Scaling exponent γ for a range of K. Note that in computing γ, the same range of D values was used for all K values.

K	5	6	7	8	9	11	12	15	25
γ	0.52	0.76	0.80	0.98	0.96	0.95	0.86	0.90	0.91

its saturation value clearly depend on the value of the diffusivity D.

These four stages have been universal to our investigations of persistent patterns, in maps as well as flows, and across the board for initial conditions and parameters. We argue that this constancy of χ^2 arising through these preliminary stages, and corresponding explicitly to the physical mechanism of the competition between chaos and diffusion, is the unambiguous dynamical signature for persistent patterns.

We now turn to the relationship between the scaling of the constant or asymptotic value of χ with diffusion strength; as we argue, this serves as a probe of the phase-space structures of the diffusion-free chaotic advection.

III. MULTIFRACTALITY IN PERSISTENT PATTERNS

As shown in the inset in Fig. 2(a), the saturation value scales as $D^{-\gamma}$ over several decades for a range of D values. This is, in itself, remarkable. That is, while it is intuitive that there is a balance between chaos and diffusion in the production of persistent patterns, a scaling relationship is not entirely obvious. Since larger values of D probe finer scales in phase space, the existence of this scaling means that there must be a specific self-similarity between distributions of phase-space structures at different scales.

As we know, the phase-space structure is a measure of the chaoticity of the problem, and Table I clearly shows that the relevant value of γ depends on the nature of the phase space. Specifically, (i) $\gamma \to 0.5$ when the dynamics is dominated by large stable structures or boundary layers associated with them as in the $K \simeq 5$ regime, (ii) $\gamma \to 1$ as one approaches the uniformly hyperbolic case, $K \geq 50$, and (iii) $1/2 < \gamma < 1$ in a nonmonotonic manner for intermediate values of K.

To understand this, we first need to identify the time scales on which the steady state arises. We start with a consideration of the transition between regions (A) and (B), namely, the time beyond which new structure formed by the dynamics is eliminated by diffusion. The details of this analysis are in Ref. [8]. The basic idea is to consider the evolution of noisy trajectories, specifically the changes in orientation of unstable and stable directions due to the noise. Instantaneous averages over realizations of these trajectories results in a transverse smoothing over widths $l_T \approx \sqrt{Dt}$. In a compact phase space, this implies that noise will homogenize structures on scales finer than l_T. The time associated with this can be estimated by considering an initially small compact region of phase-space area u_0^2. If the trajectory is bounded within a phase-space area A, the typical separation of neighboring folds of the trajectory is estimated by $\delta(t) \approx A/(u_0 e^{\lambda t})$, where λ is the Lyapunov exponent. The time

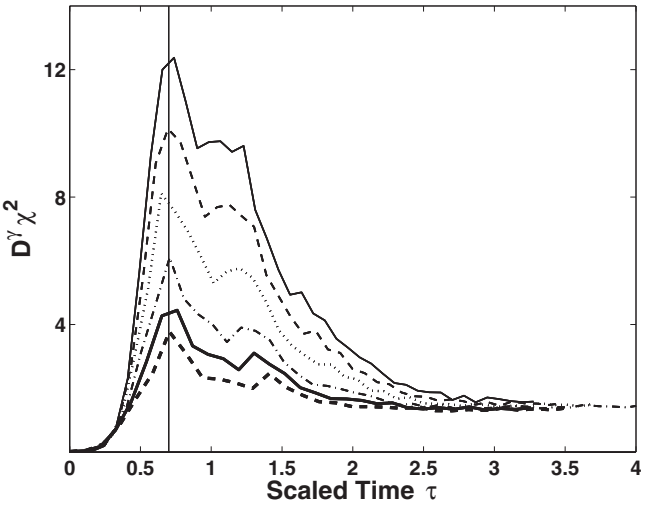

FIG. 3. χ^2 scaled by the $D^{-\gamma}$ and time scaled by $\ln 1/D$ plotted for $K=2.1$ and values of D from 5×10^{-6}–10^{-4}. The higher values of scaled χ^2 correspond to smaller D.

beyond which any new structures will be smoothed over is given by setting $l_T = \delta(t)$. An approximate solution to this transcendental equation gives

$$t^* \simeq \frac{x_0}{2\lambda}\left[1 - \frac{\ln(x_0)}{1+x_0}\right], \tag{8}$$

where $x_0 = \ln[2\lambda A^2/(Du_0^2)]$. The leading behavior $\ln(1/D)$ scaling of the time to peak $\chi^2(t)$ is clearly seen in Fig. 3 where, for fixed K and varying D, both the time for termination of structure (peak of the χ^2 curve) and χ^2_∞ scale as expected.

Beyond this time, nonuniformity in the dynamics lead to secondary peaks and, ultimately, the saturation value of χ^2 at which point the production and elimination of structure (over a period of the periodic forcing) counterbalance. Thus, the scaling exponent γ is expected to be a function of the nonuniformity in the phase space. This is clearly supported by the limiting case of the uniformly hyperbolic Arnold Cat map where the unstable manifold (wrapped around the torus) consists of straight lines which, after a few iterations, become equally spaced. Thus, diffusion (which acts along strong gradients, hence effectively transverse to the manifolds) can smooth out all the structure simultaneously once $\sqrt{Dt}$ is greater than the dynamically imposed spacing. For a more general situation such as that considered here, the spacing is strongly nonuniform. Specifically, given that the nonuniformity is what prevents the diffusive term from effectively homogenizing the concentration field, it is sensible to attempt to relate γ to measures reflecting this heterogeneity in phase space.

The multifractal formalism provides an effective way to gauge "clumping" on a range of scales [16,18]. To obtain a measure of this clumping, we need to consider the so-called $f(\alpha)$ spectrum of singularities for the dynamics. To do this, we begin by generating 10^6 points [pairs of (q,p)] in phase space by iterating the standard map. The singularity strength α_i is then defined by $P_i(l) \sim l^{\alpha_i}$, where the set of points is

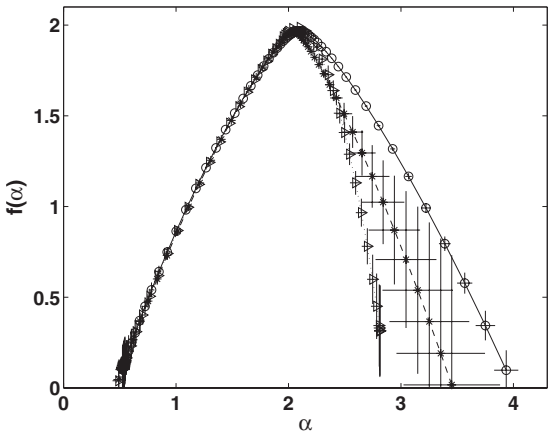

FIG. 4. Singularity spectrum with error bars for $K=7$ (circles, solid line), $K=9$ (triangles, dotted line), and $K=12$ (crosses, dashed line). The values of γ are 0.8, 0.96, and 0.86, respectively.

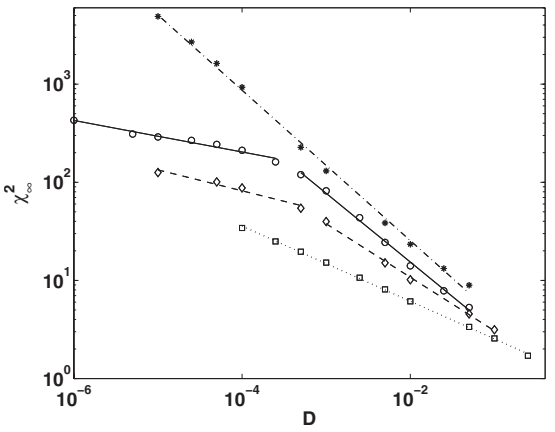

FIG. 5. Saturation value χ^2_∞ over a wider range of diffusivity D, exhibiting different scaling over ranges of diffusivity. Parameter values shown are $K=4.5$ (squares), $K=5.5$ (diamonds), $K=6$ (circles), and $K=7$ (asterisks).

covered by boxes of size l and $P_i(l)$ is the probability to be in the ith boxes. α_i can take on a range of values depending on the scale of regions being explored. The number of boxes $N(\alpha)$ which have singularity strengths $(\alpha, \alpha+d\alpha)$ scale as $N(\alpha) \sim l^{-f(\alpha)}$. $f(\alpha)$ is related to generalized dimensions D_q defined by [16,18]

$$D_q = \frac{1}{(q-1)} \lim_{l \to 0} \frac{\ln\left[\sum_i P_i^q(l)\right]}{\ln(l)}, \tag{9}$$

where $D_{q=0} \equiv H_D$, the usual Hausdorff dimension. $f(\alpha)=0$ corresponds to the limiting cases of $D_{\pm\infty}$. The above definition of D_q is constructive [18] and is what we use to compute the $f(\alpha)$ spectrum.

Figure 4 shows the singularity spectra for three cases chosen from Table I to highlight the nonmonotonic variation in the exponent γ with K. In terms of the $f(\alpha)$ curve, the difference in α values corresponding to $D_{\pm\infty}$ reflects the nonuniformity in the way map iterates fill phase space. The figure clearly illustrates that smaller γ correlates with a wider range of singularity strengths, which means nonuniformity on multiple scales. This is consistent with the fact that smaller values of γ are indicative of the diminished ability of diffusion in homogenizing the scalar field. By contrast, the $K=9$ case, with the largest value of γ, is significantly narrower. Differences in the singularity spectra are confined to the finer scales. We thus see that multifractality is reflected directly in γ.

The width in the $f(\alpha)$ curves reflects the fact that there are structures in phase space on multiple scales. In the case of the standard map, it is well known that, even for very large values of the stochasticity parameter K, islands of stability exist which, in turn, generate nonuniformity in the otherwise hyperbolic map dynamics. Of course, the value of the diffusivity effectively sets a lower bound on dynamically relevant length scales.

In an effort to understand the role played by smaller local structures with changing diffusive length scales, we further probed the scaling of χ^2_∞ over a wider range of D as shown in Fig. 5. For the specific case of $K=6$ (solid line), there are clearly two regimes where lower D values are less effective in eliminating scalar gradients as reflected in a change in slope to a significantly smaller value of γ. By contrast, we note that both larger and smaller values of K are characterized by a single slope in Fig. 5.

We first present preliminary results exploring the origins of the two-slope behavior. Figure 6 shows a magnified portion of the classical phase space corresponding to $K=6$ centered on one of two small stable regions. Our results suggest that, for values of D small enough to resolve this structure, the persistent patterns are linked to local, rather than global, aspects of the phase space. In this case, the stable region is less susceptible to the effects of diffusion. This explanation is further supported by the case of $K=5.5$ shown in Fig. 5. Here, too, the islands seen for $K=6$ exist but now occupy a slightly larger fraction of phase space—thus suggesting two-slope behavior with the break at a larger D value, which is precisely what is seen. However, on decreasing to $K=4.5$,

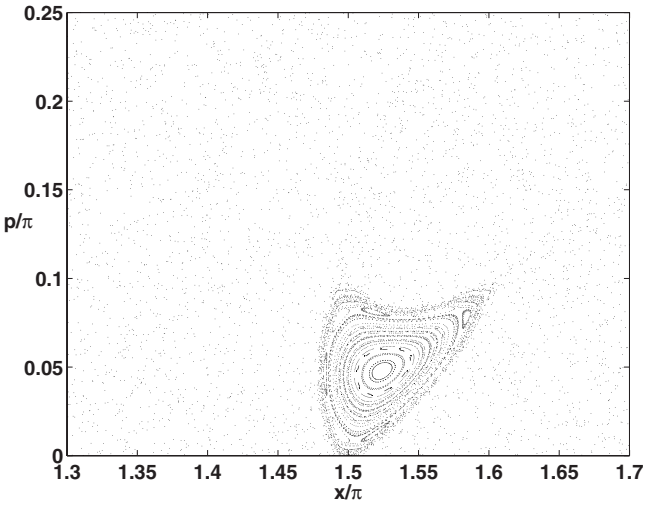

FIG. 6. Part of the classical phase space for $K=6$ showing the presence of a small stable region. Note that a symmetric partner also exists elsewhere.

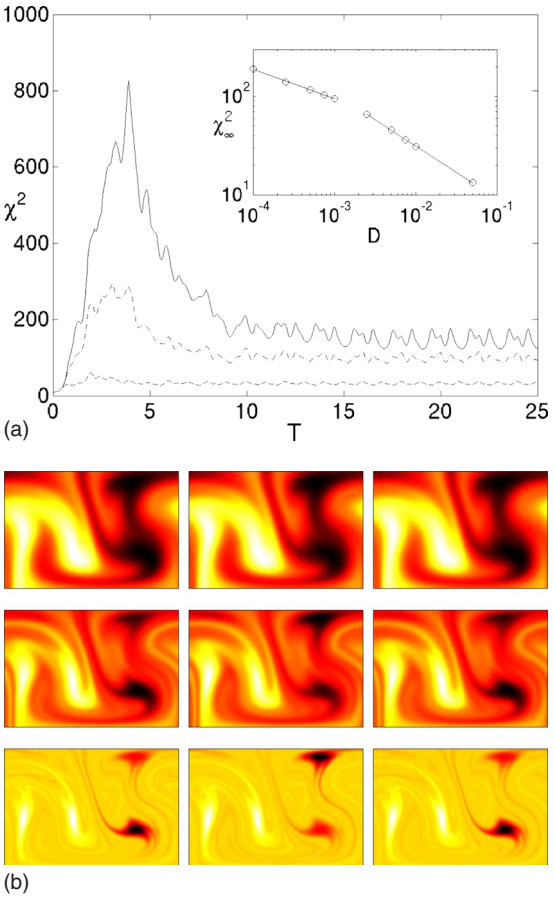

FIG. 7. (Color online) (a) $\chi^2(t)$ for the advection diffusion equation for the sin-sin flow; $\omega=0.25$, $\varepsilon=0.35$. $D=2.5\times10^{-4}$ (solid), $D=10^{-3}$ (dot-dashed), and $D=10^{-2}$ (dashed). Time measured in periods of the velocity field. Inset: saturation value of χ^2 as a function of D; (b) persistent patterns for the three diffusivities (diffusivity decreasing from the top) at three different periods: $T=22$ (left), $T=23$ (middle), and $T=24$ (right).

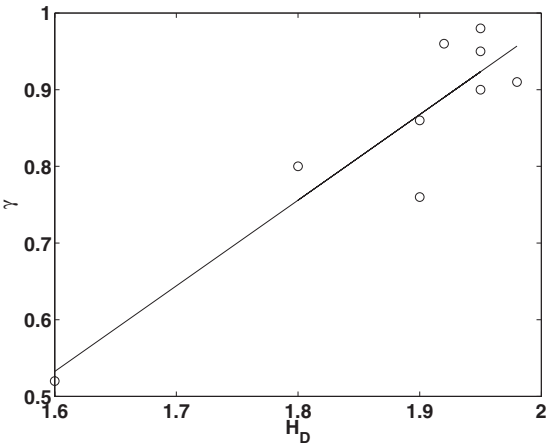

FIG. 8. Scaling exponent γ plotted against the corresponding finite-time Hausdorff dimension, H_D. The straight line is a fit drawn primarily to guide the eyes.

where the scale of the stable regions is comparable to those associated with the unstable one (e.g., lobe areas), we return to a single scaling exponent across a wide range of D.

It should be noted here that by picking appropriate initial conditions, i.e., those that have no projection onto the stable regions, one can return to a single scaling exponent. The initial condition used, in our case, extends over the entire allowed region and the range of D values used in constructing Table I straddled both regions seen in Fig. 5. We believe that the smaller value of γ seen is a direct consequence of mixed phase-space effects. The general validity of this relationship as well as the transition from global to local in phase space clearly merits more detailed exploration.

To explicitly verify that these results carry over to time-continuous vector fields, we have examined the behavior of $\chi^2(t)$ for a number of time-periodic flow fields, including those produced by dynamically consistent solutions of the 2D Navier-Stokes equation. In complete correspondence to the mixed phase-space solutions of the standard map, the dynamics of $\chi^2(t)$ for all flows considered show the same stages of evolution as well as power-law scaling of the saturation value with diffusivity for the range of diffusivities amenable to numerical investigation.

The top panel of Fig. 7 shows χ^2 behavior for the stream function $\psi(x,y,t)=-c_1y+\sin(k_1x)\sin(l_1y)+\varepsilon\sin(k_2x+2\pi\omega t)\sin(l_2y)$. For the parameters considered, the corresponding Poincaré map of the conservative dynamics shows two small pairs of period-2 islands embedded in a large chaotic sea. While there is very strong evidence of power-law scaling for χ^2_{sat} for all values of D considered, the inset indicates that the scaling exponent is quite different for small diffusivities compared to that obtained for intermediate values. As the plots of the scalar field show, the difference between these two regimes is directly linked to the periodicity of the corresponding eigenstate (persistent pattern). For larger diffusivities [see top row of Fig. 7(b)], the diffusive transport between the islands homogenizes the structure producing an eigenstate with period 1. For small enough values of the diffusivity, however, island pairs are preserved in the phase space, and eigenstates with period-2 result as seen in the bottom row of Fig. 7(b). These states are apparently much less sensitive to the level of diffusivity with the exponent γ flattening from -0.53 to -0.30. The middle row of concentration patterns is for the transition value, $D=2.5\times10^{-3}$, and indicates a weak period-2 signal in the persistent state.

Our analysis thus far has concentrated on relating conservative phase-space measures computed in the absence of diffusion to the scaling of diffusive scalars. We have yet to account for the diffusivity imposed time scale estimated earlier from considering average spacings between manifold segments. In a more speculative vein, we now extend this analysis to consider the finite-time Hausdorff dimension, H_D, computed from a finite time-time trace of the unstable manifold which provides the spatial skeleton for observed persistent patterns. An estimate of the time over which this trace needs to be considered is provided by t^* and is approximately 8–11 kicks for parameters considered. Explicitly, what is done is that the exceptional set corresponding to the unstable manifold is calculated for a finite number of iterations up to time t^* [17]. The Hausdorff dimension of this set is then

computed. We note that in the limiting case of $D \to 0$, this would lead to the usual long time "fat fractal" limit of uniform filling [19].

Figure 8 plots the exponent γ, taken from Table I, against the corresponding values (based on K) of H_D computed as described above. We note that the limits of uniformly hyperbolic, $H_D=2$, $\gamma=1$, and fully integrable dynamics, $H_D=1$, $\gamma=0$, would be consistent with a linear relationship of the form $\gamma=H_D-1$. The fit shown in the figure does not match this well but suggests the need for a more detailed study involving (a) a wider range of stochasticity values, (b) an estimation of error in both γ and H_D, and, perhaps most critically, (c) an assessment of the dependence of the finite time H_D to the choice of t^*.

IV. CONCLUDING REMARKS

In conclusion, we have demonstrated using a simple measure, $\chi^2(t)$, that competition between non-uniformly-hyperbolic structure-producing dynamics and the homogenizing diffusion is necessary for the formation of persistent patterns. There are distinct and universal characteristic dynamical stages through which χ^2 progresses before entering the persistent pattern regime. Further, scaling arguments suggest a relationship between nonuniformity in phase space and the efficacy of diffusion in eliminating density gradients. Preliminary results shown suggest that this may be explicitly demonstrated using measures reflecting the multifractal nature of the dynamics. Though our results were obtained by using a dynamical map, we have verified that all our findings apply equally well to continuous flows. We note that the above emphasizes that even for the simplest flows the subtle interplay between phase-space geometry and diffusive smoothing makes the analysis of the asymptotics of vanishing diffusivity very difficult [12].

ACKNOWLEDGMENTS

A.C.P. was supported in part under Grants No. ONR-140410192 and No. PSC-CUNY 69629-0038. A.K.P. acknowledges support from Carleton College through the Sit, Wallin, and Class of 1949 fund.

[1] H. Aref, J. Fluid Mech. **143**, 1 (1984); J. M. Ottino, *The Kinematics of Mixing: Stretching, Chaos, and Transport* (Cambridge University Press, New York, 1989); Phys. Fluids A **3** (5), 1009 (1991), special issue of the Proceedings of the IUTAM Symposium on Fluid Mechanics of Stirring and Mixing.
[2] R. T. Pierrehumbert, Chaos, Solitons Fractals **4**, 1091 (1994).
[3] D. Rothstein, E. Henry, and J. P. Gollub, Nature (London) **401**, 770 (1999).
[4] G. A. Voth, G. H. Haller, and J. P. Gollub, Phys. Rev. Lett. **88**, 254501 (2002).
[5] J. Sukhatme and R. T. Pierrehumbert, Phys. Rev. E **66**, 056302 (2002).
[6] J. L. Thiffeault, Chaos **14**, 531 (2004).
[7] O. V. Popovych, A. Pikovsky, and B. Eckhardt, Phys. Rev. E **75**, 036308 (2007).
[8] B. D. Greenbaum, S. Habib, K. Shizume, and B. Sundaram, Phys. Rev. E **76**, 046215 (2007).
[9] T. M. Antonsen, Z. C. Fan, E. Ott, and E. Garcia Lopez, Phys. Fluids **8**, 3094 (1996).
[10] E. Balkovsky and A. Fouxon, Phys. Rev. E **60**, 4164 (1999).
[11] D. R. Fereday and P. H. Haynes, Phys. Fluids **16**, 4359 (2004).
[12] Y. K. Tsang, E. Ott, T. M. Antonsen, and P. N. Guzdar, Phys. Rev. E **71**, 066313 (2005).
[13] P. H. Haynes and J. Vanneste, Phys. Fluids **17**, 097103 (2005).
[14] M. Giona, A. Adrover, S. Cerbelli, and V. Vitacolonna, Phys. Rev. Lett. **92**, 114101 (2004); M. Giona, A. Adrover, and S. Cerbelli, Physica A **348**, 37 (2005).
[15] A. K. Pattanayak, Physica D **148**, 1 (2001).
[16] T. C. Halsey, M. H. Jensen, L. P. Kadanoff, I. Procaccia, and B. I. Shraiman, Phys. Rev. A **33**, 1141 (1986).
[17] Time-dependent effective dimensions have been considered in other contexts, see, for example, G. Károlyi and T. Tél, Phys. Rev. Lett. **95**, 264501 (2005).
[18] A. Chhabra and R. V. Jensen, Phys. Rev. Lett. **62**, 1327 (1989); A. B. Chhabra, C. Meneveau, R. V. Jensen, and K. R. Sreenivasan, Phys. Rev. A **40**, 5284 (1989).
[19] D. K. Umberger and J. D. Farmer, Phys. Rev. Lett. **55**, 661 (1985).